

Formation of NaH Molecules in the Lowest Rovibrational Level of the Ground Electronic State via Short-Range Photoassociation

Jinglun Li, Yin Huang, Ting Xie, Shuo Chai and Shulin Cong*

School of Physics and Optoelectronic Technology, Dalian University of Technology, Dalian 116024, China.

Received 1 November 2013; Accepted (in revised version) 3 June 2014

Abstract. The formation of NaH molecules in the lowest rovibrational level of the ground electronic state is investigated using a pump-dump photoassociation (PA) scheme. In short-range region, two colliding atoms Na and H are efficiently associated into the NaH molecule in the rovibrational $|0,0\rangle$ state of the ground electronic state via the intermediately rovibrational $|10,1\rangle$ state of the excited electronic state. The changes of populations with the electric field amplitudes, frequency detunings, dump pulse duration and delay time between two laser pulses are calculated and discussed. The PA probability reaches 0.623 with a high state-selectivity.

PACS: 34.50.Rk, 82.20.Bc, 82.50.Nd, 82.30.Nr

Key words: Short-range photoassociation, NaH molecule, rovibrational state.

1 Introduction

In recent years, the control of atomic and molecular processes with ultrashort laser pulses has made considerable progress, including photoassociation (PA) [1–4], photodissociation [5–10] and laser-control of molecular orientation [11–15]. In a PA process, external laser field induces colliding atoms to associate into molecules. The PA process of cold ($T < 1$ K) or ultracold ($T < 1$ mK) alkali-metal atoms taken place in a long internuclear range ($2 < R < 20000 a_0$, where a_0 is Bohr radius) has recently been widely investigated by using the shaped and chirped laser pulse techniques [16–22]. And a small number of research works have focused on the short-range ($R < 30 a_0$) PA process of atoms at high temperature ($T > 1$ K) [23–32]. The short-range PA at high temperature

*Corresponding author. *Email addresses:* jinglunli@mail.dlut.edu.cn (J. Li), yinhuang@mail.dlut.edu.cn (Y. Huang), xieting@mail.dlut.edu.cn (T. Xie), chaishuo@dlut.edu.cn (S. Chai), shlcong@dlut.edu.cn (S. Cong)

is a more challenging and significance research topic in physics and chemistry. Engel and co-workers studied the PA reaction driven by the shaped laser pulse using the local control theory [23,24]. Kosloff and co-workers focused their attention on the PA process of thermally hot atoms [25,26]. Korolkov *et al.* investigated theoretically the vibrational sate-selectivity PA reaction [27]. de Lima *et al.* calculated the PA probability using one-dimensional wave-packet method [28,29]. We investigated theoretically the PA and photodissociation processes driven by the femtosecond and picosecond laser pulses [30–32].

How to produce stable photoassociated molecules is an important topic in the quantum control research field [24,33], since the PA molecules in the lowest rovibrational level of the ground electronic state are the most stable ones. Up to now, most of theoretical schemes for PA processes only study the control of vibrational states, and not take rotational states into account. In the present work, we study the short-range PA process to prepare the NaH molecule in the lowest rovibrational state of the ground electronic state by using a pump-dump PA scheme including two electronic states and the vibrational and rotational degrees of freedom. The numerical simulation shows that a high PA yield can be achieved using this simple PA scheme.

2 Theoretical calculation methods

In the PA process of Na and H atoms, the Hamiltonian describing the transition from the ground $X^1\Sigma^+$ electronic state to the excited $A^1\Sigma^+$ electronic state can be expressed as

$$\hat{\mathbf{H}}(t) = \begin{pmatrix} \hat{T}(R,\theta) + V_g(R) + W_{11}(R,\theta,t) & W_{12}(R,\theta,t) \\ W_{21}(R,\theta,t) & \hat{T}(R,\theta) + V_e(R) + W_{22}(R,\theta,t) \end{pmatrix}, \quad (2.1)$$

where R is the internuclear distance and θ the angle between the laser polarization and the molecular axis. $V_g(R)$ and $V_e(R)$ denote the potentials of the ground $X^1\Sigma^+$ and excited $A^1\Sigma^+$ electronic states, respectively. The kinetic energy operator $\hat{T}(R,\theta)$ is given by

$$\hat{T}(R,\theta) = \hat{T}_k + \hat{T}_\theta \quad (2.2)$$

with

$$\hat{T}_k = -\frac{\hbar^2}{2m} \frac{\partial^2}{\partial R^2} \quad (2.3)$$

and

$$\hat{T}_\theta = -\frac{\hbar^2}{2mR^2} \frac{1}{\sin\theta} \frac{\partial}{\partial\theta} \left(\sin\theta \frac{\partial}{\partial\theta} \right), \quad (2.4)$$

where m is the reduced mass of the NaH molecule. The laser-molecule interaction Hamiltonian $W_{ij}(R,\theta,t)$ is expressed as

$$W_{ij}(R,\theta,t) = -\mu_{ij}(R)\varepsilon(t)\cos\theta, \quad (2.5)$$

where $\mu_{ij}(R)$ denote the dipole moment matrix elements of the NaH molecule. In the calculation, $V_g(R)$ and $V_e(R)$ are adopted from Ref. [34], and $\mu_{ij}(R)$ are taken from Refs. [34, 35]. The total electric field $\varepsilon(t)$ of the pump and dump pulses is given by

$$\varepsilon(t) = \varepsilon_1 \exp \left[-4 \ln 2 \left(\frac{t - t_{p1}}{\tau_1} \right)^2 \right] \cos(\omega_1 t) + \varepsilon_2 \exp \left[-4 \ln 2 \left(\frac{t - t_{p2}}{\tau_2} \right)^2 \right] \cos(\omega_2 t), \quad (2.6)$$

where ε_i , t_{p_i} , τ_i and ω_i are the electric field amplitude, central time, duration and central frequency of the i th pulse in order. The first and second pulses are referred to as pump and dump pulses, respectively. The time-dependent Schrödinger equation of the PA process is expressed as

$$i\hbar \frac{\partial}{\partial t} |\Psi(t)\rangle = \hat{\mathbf{H}}(t) |\Psi(t)\rangle \quad (2.7)$$

with a two-component wave function

$$\Psi(t) = \begin{pmatrix} \psi_1(R, \theta, t) \\ \psi_2(R, \theta, t) \end{pmatrix}, \quad (2.8)$$

where $\psi_1(R, \theta, t)$ and $\psi_2(R, \theta, t)$ are the wave functions of the ground $X^1\Sigma^+$ and excited $A^1\Sigma^+$ electronic states, respectively. The angular part of the wave function is taken to be normalized Legendre polynomials [31]. The initial state is the continuum state of the ground electronic state and can be described by the Gaussian wave packet

$$\Psi(R, \theta, 0) = \begin{pmatrix} \left(\frac{2}{\pi\sigma^2} \right)^{1/4} \times P_l(\cos\theta) \exp \left[ik_0 R - \left(\frac{R - R_0}{\sigma} \right)^2 \right] \\ 0 \end{pmatrix}, \quad (2.9)$$

where σ denotes the width of the initial wave packet. R_0 and k_0 are the center location and momentum of the initial wave packet, respectively. The collision energy E is given by

$$E = \frac{\hbar^2}{2m} \left(k_0^2 + \frac{1}{\sigma^2} \right). \quad (2.10)$$

The time-dependent Schrödinger equation is solved by using the split operator method [31, 36]. For a short time step δ in the propagation, the wave function at $t + \delta$ can be derived from $\Psi(t)$ as follows,

$$\Psi(t + \delta) = \exp \left(\frac{-i\delta \hat{T}_k}{2\hbar} \right) \exp \left(\frac{-i\delta \hat{T}_\theta}{2\hbar} \right) \exp \left(\frac{-i\delta V}{\hbar} \right) \exp \left(\frac{-i\delta \hat{T}_\theta}{2\hbar} \right) \exp \left(\frac{-i\delta \hat{T}_k}{2\hbar} \right) \Psi(t), \quad (2.11)$$

with V being defined as

$$V = \begin{pmatrix} V_g(R) + W_{11}(R, \theta, t) & W_{12}(R, \theta, t) \\ W_{21}(R, \theta, t) & V_e(R) + W_{22}(R, \theta, t) \end{pmatrix}. \quad (2.12)$$

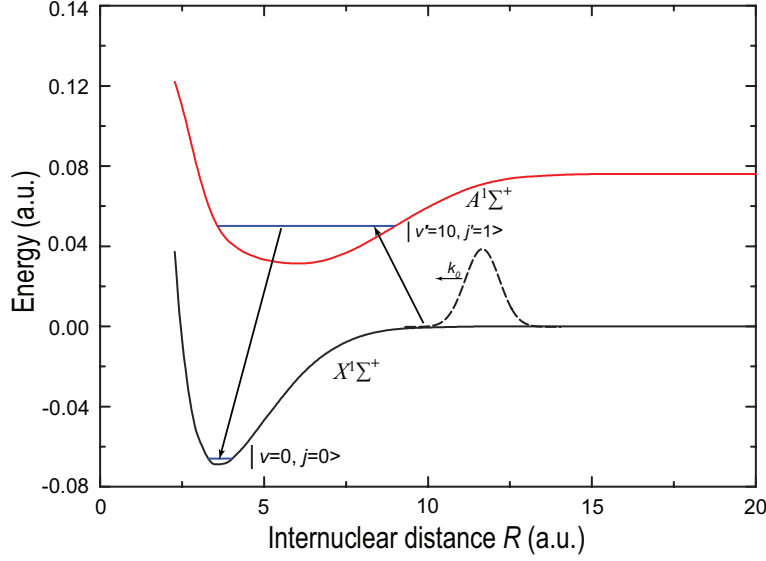


Figure 1: (Color online) The pump-dump PA scheme. The colliding atoms Na and H are excited by the pump pulse to form a unstable NaH molecule in the rovibrational $|10,1\rangle$ state of the excited $A^1\Sigma^+$ electronic state, and then is transferred to the rovibrational $|0,0\rangle$ state of the ground $X^1\Sigma^+$ electronic state by the dump pulse to form a stable NaH molecule.

The rovibrational populations are given by

$$P_{v,j}(t) = |\langle v,j | \psi_1(R,\theta,t) \rangle|^2, \quad (2.13)$$

$$P'_{v',j'}(t) = |\langle v',j' | \psi_2(R,\theta,t) \rangle|^2, \quad (2.14)$$

where the $|v,j\rangle$ and $|v',j'\rangle$ are the rovibrational eigenstates in the ground $X^1\Sigma^+$ and excited $A^1\Sigma^+$ electronic states, respectively. The total populations in the ground and excited electronic states are calculated by $P(t) = \sum_{v,j} P_{v,j}(t)$ and $P'(t) = \sum_{v',j'} P'_{v',j'}(t)$, respectively.

In the pump-dump PA scheme, the colliding atoms Na and H are firstly associated into the NaH molecule in the intermediately rovibrational $|10,1\rangle$ state of the excited electronic state by a pump pulse, and then the associated NaH molecule is transferred into the lowest rovibrational $|0,0\rangle$ state of the ground electronic state by a dump pulse, as shown in Fig. 1.

3 Results and discussions

In the calculation, the center of the initial Gaussian wave packet is chosen to be at $R_0 = 30.5 a_0$ with $\sigma = 8.0 a_0$ and $k_0 = -2.0\hbar/a_0$. To achieve a large PA probability in the $|0,0\rangle$ state, we need to select a proper intermediate state. Figs. 2(a) and 2(b) show the maxima of the time-dependent Franck-Condon overlaps $|\langle \phi_{v,1}(R) | \psi_{1R}(R,t) \rangle|_{\max}$ and $|\langle \phi'_{v',1}(R) | \psi_{1R}(R,t) \rangle|_{\max}$ in the absence of laser pulses, where $\psi_{1R}(R,t)$ is the radical

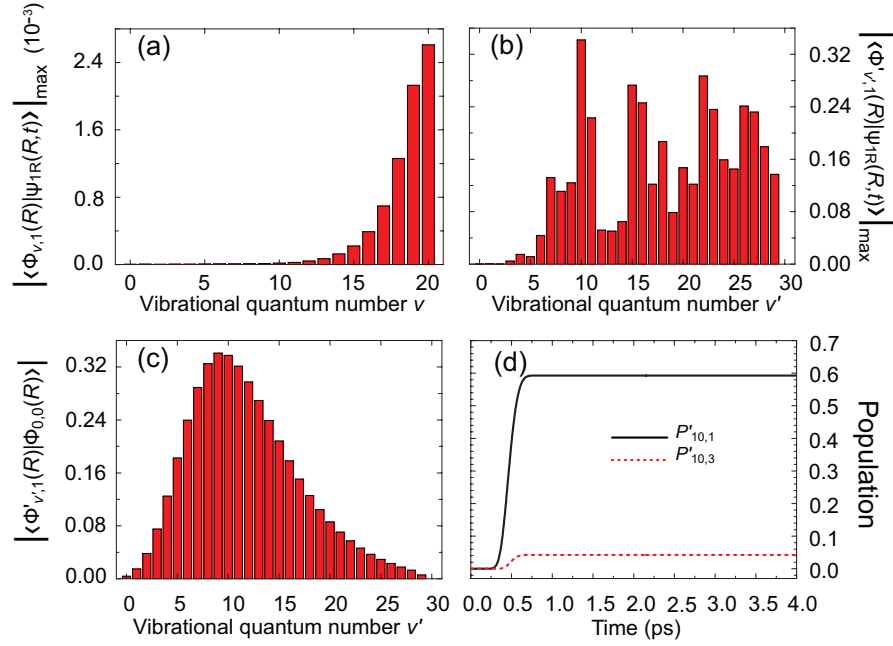


Figure 2: (Color online) (a) The Franck-Condon overlap $|\langle\phi_{v,1}(R)|\psi_{1R}(R,t)\rangle|_{\max}$ versus vibrational quantum number v . (b) The Franck-Condon overlap $|\langle\phi'_{v',1}(R)|\psi_{1R}(R,t)\rangle|_{\max}$ versus v' . (c) The Franck-Condon factor $|\langle\phi'_{v',1}(R)|\phi_{0,0}(R)\rangle|$ versus v' . (d) The populations $P'_{10,1}$ and $P'_{10,3}$ on the rovibrational $|10,1\rangle$ and $|10,3\rangle$ states of the excited $A^1\Sigma^+$ electronic state versus time. The optimized parameters of pump pulse are used: $\tau_1=0.31$ ps, $t_{p_1}=0.39$ ps, $\varepsilon_1=2.9$ MV/cm and $\Delta_{L_1}=5$ cm^{-1} .

part of $\psi_1(R,\theta,t)$. $\phi_{v,j}(R)$ and $\phi'_{v',j'}(R)$ are the radical wave functions corresponding to the $|v,j\rangle$ and $|v',j'\rangle$ states. The Franck-Condon overlaps in Fig. 2(b) are larger than those in Fig. 2(a) by two orders of magnitude. Since the transition probability depends on the Franck-Condon overlaps, we can select an intermediate state from the rovibrational states of the excited electronic state. Fig. 2(c) shows the Franck-Condon factors $|\langle\phi'_{v',1}(R)|\phi_{0,0}(R)\rangle|$, corresponding to the transition probability from the $|v',j'\rangle = |v',1\rangle$ state to the $|v,j\rangle = |0,0\rangle$ state. From Figs. 2(a-c), it can be seen that the rovibrational $|v',j'\rangle = |10,1\rangle$ state of the excited electronic state is a proper intermediate state for the pump-dump PA process, owing to the larger Franck-Condon factor. The colliding atoms Na and H are associated into the NaH molecule in the intermediately rovibrational $|10,1\rangle$ state by the pump pulse. The maximal population $P'_{10,1}$ of the intermediate state reaches 0.593, as shown in Fig. 2(d), where the optimized parameters of the pump pulse are used: duration $\tau_1=0.31$ ps, central time $t_{p_1}=0.39$ ps, electric field amplitude $\varepsilon_1=2.9$ MV/cm and detuning $\Delta_{L_1}=5$ cm^{-1} . The detuning Δ_{L_1} is defined as the deviation, ω_1-f_1 , where f_1 is the resonant frequency between the initial and intermediate states. The ratio $P'_{10,1}/P'=0.93$, indicating that 93% of population is transferred to the intermediate $|10,1\rangle$

state. The remainder is mostly distributed on the $|10,3\rangle$ state of the excited electronic state, as shown in Fig. 2(d).

By fixing the optimized parameters of the pump pulse, the parameters of the dump pulse are optimized as follows: $\tau_2 = 1.14$ ps, $t_{p_2} = 1.95$ ps, $\varepsilon_2 = 1.0$ MV/cm and $\Delta_{L_2} = -1$ cm^{-1} . Here, $\Delta_{L_2} = \omega_2 - f_2$, where f_2 is the resonant frequency from the intermediate state to the final state. Fig. 3(a) shows the electric fields of the pump and dump pulses. Fig. 3(b) illustrates the population transfer process from the ground electronic state to the excited electronic state steered by the optimized pump and dump pulses. In the time range of $[0.2, 0.7]$ ps, under the action of pump pulse, the colliding atoms Na and H are excited from the initially atomic state to the intermediately rovibrational $|10,1\rangle$ state of the NaH molecule, leading to the drastic decrease of atomic population in the initially electronic state and the rapid increase of molecular population in the rovibrational $|10,1\rangle$ state of the excited electronic state. In the time range of $[0.7, 0.8]$ ps, the populations on the ground and excited electronic states are nearly unchanged due to very low intensities of the pump and dump pulses. When $0.8 < t < 1.3$ ps, the population on the ground electronic state decreases rapidly because of the absorbing boundary condition. With the increase of dump pulse intensity, a little population is transferred from the excited electronic state to the ground electronic state, which causes the population on the excited state to decrease slightly. When $1.3 < t < 3.0$ ps, under the action of dump pulse, the population on the excited electronic state decreases while that on the ground electronic state increases. Finally, after $t = 3.0$ ps, the total population on the ground electronic state reaches a stable value, 0.634.

Fig. 3(c) illustrates the time-dependent populations of the relevant rovibrational states in the pump-dump PA process. The population $P_{0,0}$ of the NaH molecule in the lowest rovibrational $|0,0\rangle$ state is equal to 0.623. This value is larger than $P'_{10,1}$ but smaller than $P'_{10,1} + P'_{10,3}$ because a part of $P'_{10,3}$ is also transferred to the $|0,0\rangle$ state by the dump pulse via the pathway $|10,3\rangle_{\text{excited}} \xrightarrow{\hbar\omega_2} |0,2\rangle_{\text{ground}} \xrightarrow{\hbar\omega_2} |10,1\rangle_{\text{excited}} \xrightarrow{\hbar\omega_2} |0,0\rangle_{\text{ground}}$. The ratio $S = P_{0,0}/(P + P') = 0.98$, meaning that a high state-selectivity is achieved and the populations in other rovibrational states are negligibly small. For comparison, we also calculate the PA probability by using a one-dimensional model, where the rotational degree of freedom is excluded. Under the action of the same optimized pulses, the population of the lowest vibrational $v = 0$ state on the ground electronic state is only 0.094. The result shows that the pulse parameters optimized in the two-dimensional model do not satisfy the one-dimensional model. Then the pulses are optimized in the one-dimensional model and the population of the vibrational $v = 0$ state on the ground electronic state reaches 0.957. Compared with that in two-dimensional model, the electric field amplitudes optimized in one-dimensional model $\varepsilon_1 = 2.0$ MV/cm and $\varepsilon_2 = 0.56$ MV/cm have remarkable changes, while the other parameters share the same values both optimized in one- and two-dimensional models. The one-dimensional model can work out inspiring PA Probability and select out exact values of optimized central times, durations and central frequencies. However, the significant differences between the optimized electric field

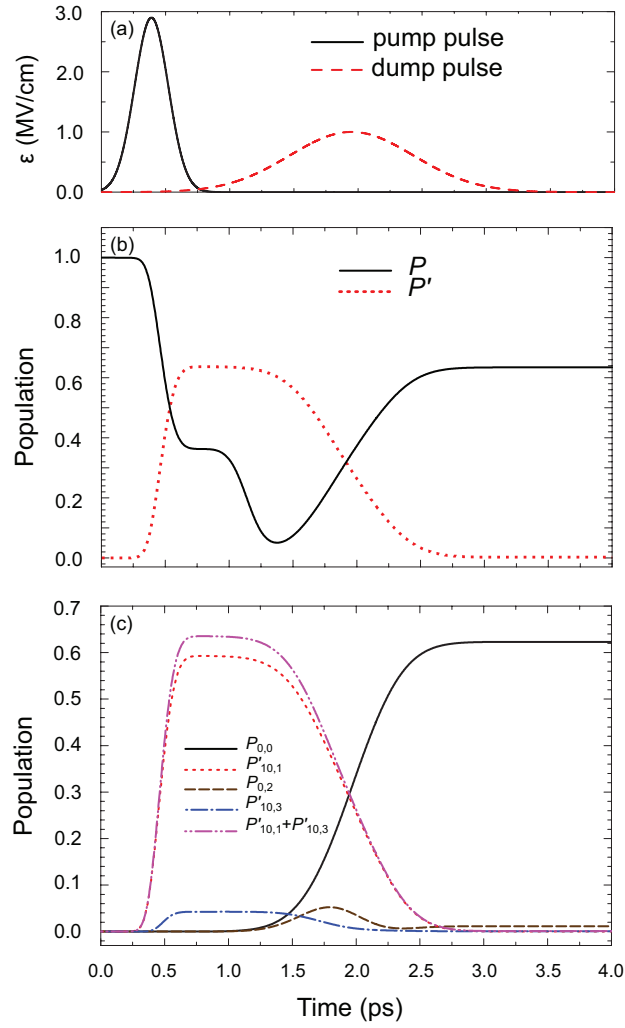


Figure 3: (Color online) (a) The optimized electric fields of the pump and dump pulses. (b) The populations P in the ground electronic state and P' in the excited electronic state versus time. (c) The populations $P_{0,0}$ and $P_{0,2}$ on the rovibrational $|0,0\rangle$ and $|0,2\rangle$ states of the ground electronic state and $P'_{10,1}$ on the $|10,1\rangle$ and $P'_{10,3}$ on the $|10,3\rangle$ states of the excited electronic state versus time. The optimized parameters of pump and dump pulses are used: $\tau_1 = 0.31$ ps, $t_{p1} = 0.39$ ps, $\epsilon_1 = 2.9$ MV/cm, $\Delta_{L1} = 5$ cm^{-1} , $\tau_2 = 1.14$ ps, $t_{p2} = 1.95$ ps, $\epsilon_2 = 1.0$ MV/cm and $\Delta_{L2} = -1$ cm^{-1} .

amplitudes of the two models indicate that the one-dimensional model is not competent to find out the accurate optimal laser pulses in our pump-dump PA scheme.

In order to investigate the influences of the electric field amplitudes ϵ_1 and ϵ_2 on the PA process, we change the amplitude ϵ_i by $\epsilon_i = \eta \epsilon_{i\text{op}}$ ($0.1 \leq \eta \leq 2.0$), where $\epsilon_{i\text{op}}$ is the optimized electric field amplitude of the i th pulse. For simplicity, we use M' and $M'_{10,1}$ to label the total population of the excited electronic state and the population of

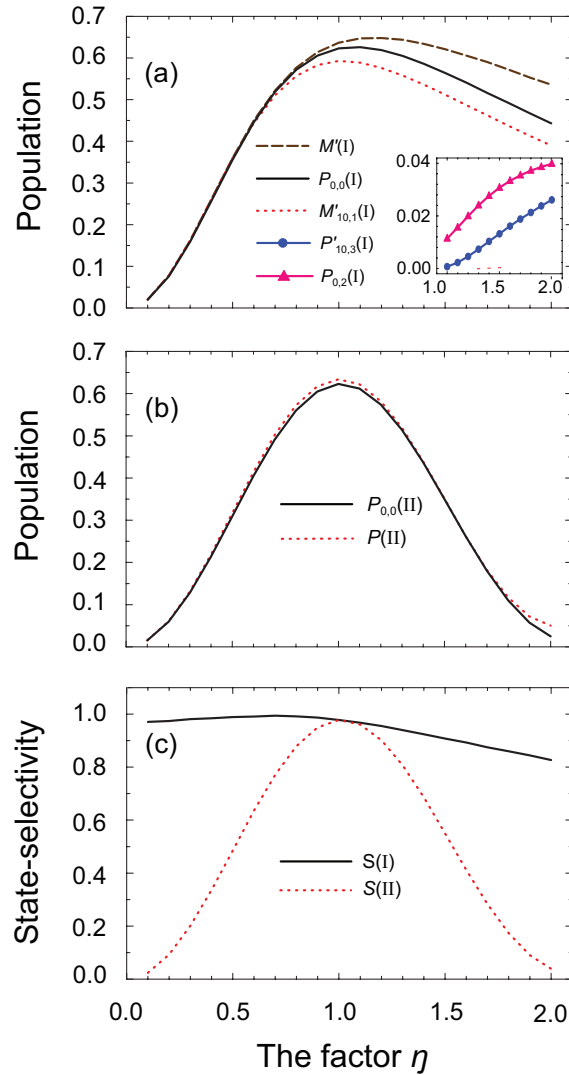


Figure 4: (Color online) The influences of the electric field amplitudes ε_1 and ε_2 on the pump-dump PA process. (a) The populations $M'(I)$, $M'_{10,1}(I)$, $P'_{10,3}(I)$, $P_{0,2}(I)$ and $P_{0,0}(I)$ versus η . (b) The populations $P(II)$ and $P_{0,0}(II)$ versus η . (c) The state-selectivity $S(I)$ and $S(II)$ versus η .

the intermediate $|10,1\rangle$ state after the pump process is over, respectively. Fig. 4 presents two cases: (I) changing ε_1 and keeping $\varepsilon_2 = \varepsilon_{2op}$ unchanged and (II) changing ε_2 while keeping $\varepsilon_1 = \varepsilon_{1op}$ unchanged. In the case (I), the populations $M'(I)$, $M'_{10,1}(I)$ and $P_{0,0}(I)$ firstly increase and then decrease, as shown in Fig. 4(a). When $\eta < 0.7$, $M'(I)$ is almost equal to $M'_{10,1}(I)$, meaning that a high state-selectivity of the intermediately rovibrational $|10,1\rangle$ state is achieved. With increasing η , the difference between $M'(I)$ and $M'_{10,1}(I)$ increases. This is because the population on the $|10,3\rangle$ state of the excited electronic state

increases with the increase of ε_1 , which lowers the state-selectivity of the $|10,1\rangle$ state. Moreover, the increase of the population on the $|10,3\rangle$ also lowers the state-selectivity of the $|0,0\rangle$ state, as shown in Fig. 4(c). This phenomenon results from the “zigzag” population transfer pathway from the $|10,3\rangle$ state to the $|0,0\rangle$ state. For each state related to the pathway, there exists residual population, and the residual effect of population is obvious especially when $\eta > 1.0$.

The inset of Fig. 4(a) shows the populations of the $|v',j'\rangle = |10,3\rangle$ and $|v,j\rangle = |0,2\rangle$ states on which a small quantity of residual population resides. It can be seen that the residual populations $P'_{10,3}(\text{I})$ and $P_{0,2}(\text{I})$ increase with the increase of η , which directly causes the state-selectivity of the $|0,0\rangle$ state to decrease. In the case (II), the populations $P_{0,0}(\text{II})$ and $P(\text{II})$ and the state-selectivity $S(\text{II})$ increase from small values to their maxima located at $\eta = 1.0$ and then decrease to small values, as shown in Figs. 4(b) and 4(c). With the increase of η , the difference between $P(\text{II})$ and $P_{0,0}(\text{II})$ is very small, and hence the population on the $|0,2\rangle$ state is negligible. When $\eta < 1.0$, the variation tendency of $P_{0,0}(\text{II})$ is similar to that of $P_{0,0}(\text{I})$. However, $P_{0,0}(\text{II})$ decreases more rapidly than $P_{0,0}(\text{I})$ with the increase of η in the range of $[1.0, 2.0]$, meaning that the variation of ε_2 changes the PA probability more drastically than that of ε_1 in strong field condition ($\eta > 1.0$). $S(\text{II})$ is more sensitive to η than $S(\text{I})$, indicating that the dump pulse has larger influence on the state-selectivity of the $|0,0\rangle$ state than the pump pulse.

In the following, the influences of the detunings Δ_{L_1} and Δ_{L_2} on the PA process are discussed. We change the detuning Δ_{L_i} by $\Delta_{L_i} = \Delta_{L_{i\text{op}}} + \Delta$ ($-20 \leq \Delta \leq 20 \text{ cm}^{-1}$), where $\Delta_{L_{i\text{op}}}$ is the optimized detuning of the i th pulse. The two cases are considered here: (A) changing Δ_{L_1} and keeping $\Delta_{L_2} = \Delta_{L_{2\text{op}}}$ unchanged and (B) changing Δ_{L_2} while keeping $\Delta_{L_1} = \Delta_{L_{1\text{op}}}$ unchanged. In the case (A), the populations $M'(\text{A})$, $M'_{10,1}(\text{A})$ and $P_{0,0}(\text{A})$ increase when $\Delta \rightarrow 0$, as shown in Fig. 5(a). The difference, $M'(\text{A}) - M'_{10,1}(\text{A})$, increases with decreasing $|\Delta|$ because of the increase of the population on the $|v',j'\rangle = |10,3\rangle$ state. Meanwhile, the difference $M'(\text{A}) - P_{0,0}(\text{A})$ increases with the decrease of $|\Delta|$. In the case (B), as shown in Fig. 5(b), $P_{0,0}(\text{B})$ varies obviously, which is different from $P_{0,0}(\text{A})$, indicating that Δ_{L_2} has stronger influence on the PA probability than Δ_{L_1} . When $-10 < \Delta < 20 \text{ cm}^{-1}$, $P(\text{B})$ is almost equal to $P_{0,0}(\text{B})$ because that the population $P_{0,2}(\text{B})$ on the $|v,j\rangle = |0,2\rangle$ state is negligible small. However, in the range of $-20 < \Delta < -10 \text{ cm}^{-1}$, $P_{0,2}(\text{B})$, describing the difference between $P(\text{B})$ and $P_{0,0}(\text{B})$, increases rapidly with the decrease of Δ . Consequently, $P(\text{B})$ decreases slower than $P_{0,0}(\text{B})$, and then increases when Δ decreases from -10 to -20 cm^{-1} . Moreover, when $\Delta < -15 \text{ cm}^{-1}$, $P_{0,2}(\text{B}) > P_{0,0}(\text{B})$. The rapid increase of $P_{0,2}(\text{B})$ can be explained by the resonance conditions of the dump pulse through channel-i and channel-ii, where channel-i presents the population transfer process from the intermediate state to the $|0,0\rangle$ state, and channel-ii presents the population transfer process from the intermediate state to the $|0,2\rangle$ state. With the decrease of Δ in the range of $[-20, -10] \text{ cm}^{-1}$, the frequency of the dump pulse approaches the resonance frequency in the channel-ii, and hence channel-ii becomes a dominant dump channel. Fig. 5(c) describes the state-selectivity of the $|0,0\rangle$ state in the cases (A) and (B). The variation of $S(\text{A})$ is negligible small, meaning that the change of Δ_{L_1} has almost no influence on the state-selectivity of

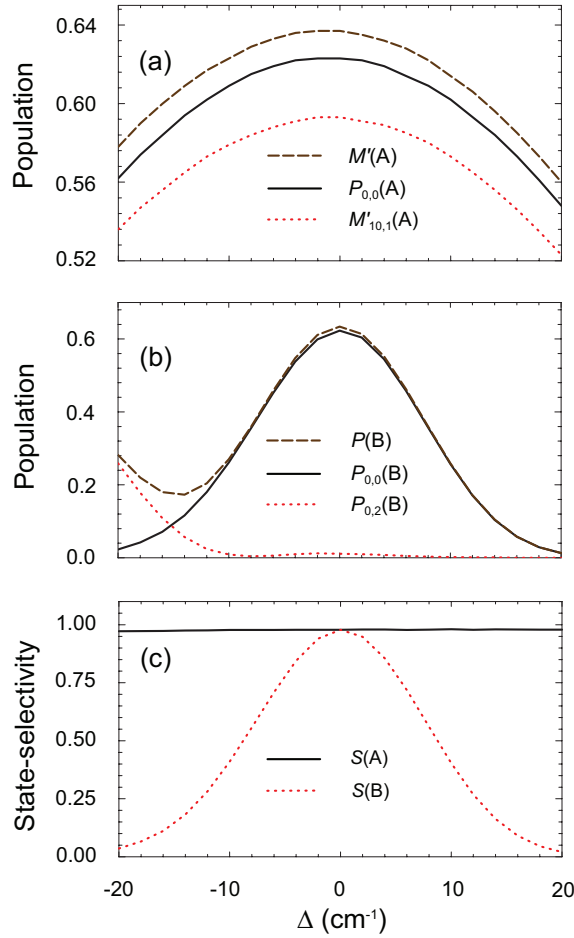


Figure 5: (Color online) The influences of the pulse frequency detunings on the PA process. (a) The populations $M'(A)$, $M'_{10,1}(A)$ and $P_{0,0}(A)$ versus Δ . (b) The populations $P(B)$ and $P_{0,0}(B)$ versus Δ . (c) The state-selectivity $S(A)$ and $S(B)$ versus Δ .

the $|0,0\rangle$ state. On the contrary, $S(B)$ varies in a large range with changing Δ_{L2} , indicating that the state-selectivity of the $|0,0\rangle$ state is sensitive to the dump frequency.

Several similar pump-dump schemes have been used to control the molecular dissociation and electronic dynamics by Lan *et al.* and Liu *et al.* [37–39]. These works inspire us to study and discuss the influences of the relative delay between the two pulses and the pulse duration which play important roles in them. We now investigate the population of the $|0,0\rangle$ state versus the delay time Δt between the two pulses, where $\Delta t = t_{p2} - t_{p1}$ by fixing $t_{p1} = 0.39$ ps. As shown in Fig. 6(a), the first maximum of the population $P_{0,0} = 0.623$ is located at $\Delta t = 1.6$ ps, which is the optimal delay time that we have studied above. Then, with the increase of Δt , the population $P_{0,0}$ oscillates periodically and the period is 1.7 ps. This oscillation is undiminished and $P_{0,0}$ reaches the same values 0.623 at the second

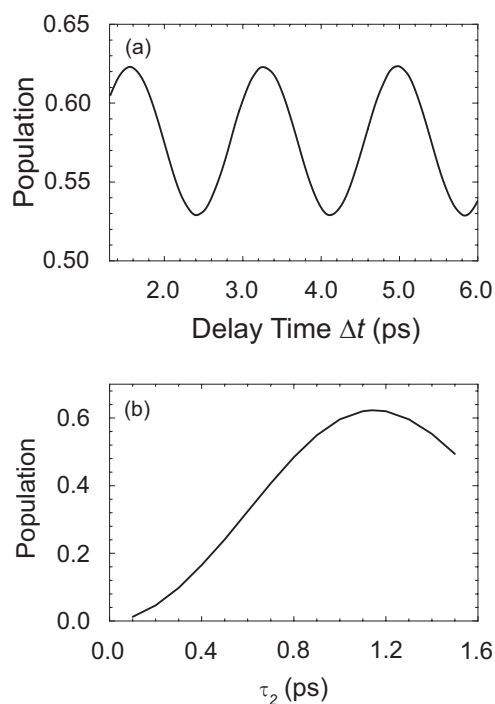


Figure 6: (Color online) (a) The population $P_{0,0}$ versus the delay time Δt . (b) The population $P_{0,0}$ versus the duration τ_2 .

($\Delta t = 3.3$ ps) and third ($\Delta t = 5.0$ ps) peaks. The minima of $P_{0,0}$ located at $\Delta t = 2.4$ and 4.1 ps share the same values, 0.529 . Notice that, with increasing Δt , the overlap of the two pulses decreases and is negligible when $\Delta t > 3.0$ ps, while the amplitude and period of the population oscillation keep unchanged, indicating the population oscillation is not induced by the change of the overlap between the two pulses. Fig. 6(b) shows the influence of the pulse duration τ_2 on the population $P_{0,0}$. It can be seen that when τ_2 is small, the pump-dump scheme is really inefficient and the population $P_{0,0}$ is small. With the increase of τ_2 , $P_{0,0}$ increases obviously and then reaches its maximal value, 0.623 , at $\tau_2 = 1.14$ ps, *ie.*, our optimized point. When the τ_2 is above 1.14 ps, the population decreases with increasing duration. Moreover, during the optimization process, we can select out the optimal τ_2 with the other parameters fixed by this way.

4 Conclusions

We have investigated theoretically how to prepare the PA NaH molecule in the lowest rovibrational level of the ground electronic state using the pump-dump PA scheme. The intermediate state is chosen to be the rovibrational $|10,1\rangle$ state of the excited electronic state due to the large Franck-Condon overlap. By optimizing the pump and dump pulses,

the population of the $|0,0\rangle$ state $P_{0,0}$ reaches 0.623 with a high state-selectivity. Compared with the one-dimensional model, the two-dimensional model can select out more accurate values of the optimal electric field amplitudes. In the pump-dump PA process, the electric field amplitude ε_2 and detuning Δ_{L_2} of the dump pulse have larger influences on the state-selectivity of the $|0,0\rangle$ state than those of the pump pulse. Moreover, the duration τ_2 and the time delay between the two pulses have important influence on the population of the $|0,0\rangle$ state.

Acknowledgments

This work was Supported by the National Natural Science Foundation of China under Grant Nos. 10974024 and 11274056.

References

- [1] A. Fioretti, D. Comparat, A. Crubellier, O. Dulieu, F. Masnou-Seeuws and P. Pillet, Formation of Cold Cs_2 Molecules through Photoassociation, *Phys. Rev. Lett.*, 80 (1998), 4402.
- [2] T. N. Nikolov, J. R. Ensher, E. E. Eyler, H. Wang, W. C. Stwalley and P. L. Gould, Efficient Production of Ground-State Potassium Molecules at Sub-mK Temperatures by Two-Step Photoassociation, *Phys. Rev. Lett.*, 84 (2000), 246.
- [3] X.-J. Hu, W. Zhang, Y. Huang, J.-F. Yang and S.-L. Cong, Formation of Ultracold Cesium Molecules in the Ground Electronic State, *J. Theor. Comput. Chem.*, 11 (2012), 1323.
- [4] A. Homer and G. Roberts, Chirped fields for Rb + Cs photoassociation, *Phys. Rev. A*, 78 (2008), 053404.
- [5] S. Chelkowski and A. D. Bandrauk, Visualizing electron delocalization, electron-proton correlations, and the Einstein-Podolsky-Rosen paradox during the photodissociation of a diatomic molecule using two ultrashort laser pulses, *Phys. Rev. A*, 81 (2010), 062101.
- [6] R. Lefebvre, O. Atabek, M. Šindelka and N. Moiseyev, Resonance Coalescence in Molecular Photodissociation, *Phys. Rev. Lett.*, 103 (2009), 123003.
- [7] Y. Liu, J. Li, J. Yu and S.-L. Cong, Field-Free Molecular Orientation in Dissipative Media by a Combination of Femtosecond and THz Laser Pulses, *J. Theor. Comput. Chem.*, 12 (2013), 1350006.
- [8] J. Yu, C.-C. Shu, W.-H. Hu and S.-L. Cong, Above Threshold Ionization of Polar NaK Molecules Driven by Few-Cycle Laser Pulse, *J. Theor. Comput. Chem.*, 9 (2010), 785.
- [9] R. Schinke, Photodissociation of N_2O : Potential Energy Surfaces and Absorption Spectrum, *J. Chem. Phys.*, 134 (2011), 064313.
- [10] K. Osawa, M. Terazima and Y. Kimura, Photo-dissociation Dynamics of Bis(p-dimethylaminophenyl) Disulfide in Ionic liquids Studied by Ultrafast Transient Absorption Spectroscopy, *Chem. Phys. Lett.*, 564 (2013), 21.
- [11] A. Goban, S. Minemoto and H. Sakai, Laser-Field-Free Molecular Orientation, *Phys. Rev. Lett.*, 101 (2008), 013001.
- [12] R. Tehini and D. Sugny, Field-free molecular orientation by nonresonant and quasiresonant two-color laser pulses, *Phys. Rev. A*, 77 (2008), 023407.
- [13] C.-C. Shu, K.-J. Yuan, W.-H. Hu and S.-L. Cong, Field-free molecular orientation with terahertz few-cycle pulses, *J. Chem. Phys.*, 132 (2010), 244311.

- [14] M. Spanner, S. Patchkovskii, E. Frumker and P. Corkum, Mechanisms of Two-Color Laser-Induced Field-Free Molecular Orientation, *Phys. Rev. Lett.*, 109 (2012), 113001.
- [15] M. Lapert and D. Sugny, Field-free molecular orientation by terahertz laser pulses at high temperature, *Phys. Rev. A*, 85 (2012), 063418.
- [16] W. Zhang, Y. Huang, T. Xie, G.-R. Wang and S.-L. Cong, Efficient photoassociation with a slowly-turned-on and rapidly-turned-off laser field, *Phys. Rev. A*, 82 (2010), 063411.
- [17] E. Luc-Koenig, R. Kosloff, F. Masnou-Seeuws and M. Vatasescu, Photoassociation of cold atoms with chirped laser pulses: Time-dependent calculations and analysis of the adiabatic transfer within a two-state model, *Phys. Rev. A*, 70 (2004), 033414.
- [18] F. Lin, W. Zhang, Z.-Y. Zhao and S.-L. Cong, Suppressing the weakly bound states in the photoassociation dynamics by using a frequency cut-off laser pulse, *Chin. Phys. B*, 21 (2012), 073203.
- [19] B. E. Londoño, J. E. Mahecha, E. Luc-Koenig and A. Crubellier, Resonant coupling effects on the photoassociation of ultracold Rb and Cs atoms, *Phys. Rev. A*, 80 (2009), 032511.
- [20] N. Bouloufa, A. Crubellier and O. Dulieu, Reexamination of the 0_g^- pure long-range state of Cs_2 : Prediction of missing levels in the photoassociation spectrum, *Phys. Rev. A*, 75 (2007), 052501.
- [21] Y. Huang, W. Zhang, G.-R. Wang, T. Xie and S.-L. Cong, Formation of $^{85}\text{Rb}_2$ ultracold molecules via photoassociation by two-color laser fields modulating the Gaussian amplitude, *Phys. Rev. A*, 86 (2012), 043420.
- [22] F. Weise, A. Merli, F. Eimer, S. Birkner, F. Sauer, L. Wöste, A. Lindinger, W. Salzmann, T. G. Mullins, R. Wester, M. Weidemüller, R. Ağanoglu and C. P. Koch, Characteristic oscillations in the coherent transients of ultracold rubidium molecules using red and blue detuned pulses for photoassociation, *J. Phys. B*, 42 (2009), 215307.
- [23] P. Marquetand and V. Engel, Local control theory applied to molecular photoassociation, *J Chem. Phys.*, 127 (2007), 084115.
- [24] P. Marquetand and V. Engel, Analysis of laser fields for photoassociation and molecular stabilization derived from local control theory, *J Phys. B*, 41 (2008), 074026.
- [25] L. Rybak, S. Amaran, L. Levin, M. Tomza, R. Moszynski, R. Kosloff, C. P. Koch and Z. Amitay, Generating Molecular Rovibrational Coherence by Two-Photon Femtosecond Photoassociation of Thermally Hot Atoms, *Phys. Rev. Lett.*, 107 (2011), 273001.
- [26] L. Rybak, Z. Amitay, S. Amaran, R. Kosloff, M. Tomza, R. Moszynski and C. P. Koch, Femtosecond coherent control of thermal photoassociation of magnesium atoms, *Faraday Discuss.*, 153 (2011), 383.
- [27] M. V. Korolkov and B. Schmidt, Spin-orbit induced association under ultrafast laser pulse control, *Chem. Phys. Lett.*, 361 (2002), 432.
- [28] E. F. de Lima, T.-S. Ho and H. Rabitz, Laser-pulse photoassociation in a thermal gas of atoms, *Phys. Rev. A*, 78 (2008), 063417.
- [29] E. F. de Lima, T.-S. Ho and H. Rabitz, Optimal laser control of molecular photoassociation along with vibrational stabilization, *Chem. Phys. Lett.*, 501 (2011), 267.
- [30] Y.-Y. Niu, S.-M. Wang and S.-L. Cong, Vibrational state-selectivity of product HI in photoassociation reaction $\text{I} + \text{H} \rightarrow \text{HI}$, *Chem. Phys. Lett.*, 428 (2006), 7.
- [31] Q.-Z. Su, J. Yu, Y.-Y. Niu and S.-L. Cong, Rovibration for Formation of Ultracold NaH Molecules Induced by an Ultrashort Laser Pulse, *Chin. Phys. Lett.*, 27 (2010), 093401.
- [32] Y.-Y. Niu, R. Wang, L. Liu and S.-L. Cong, Photoassociation Reactions $\text{H} + \text{D}^+$ and $\text{H}^+ + \text{D}$ in Ultrashort Pulse Laser Fields, *Chin. Phys. Lett.*, 24 (2007), 3400.
- [33] K. Aikawa, D. Akamatsu, M. Hayashi, K. Oasa, J. Kobayashi, P. Naidon, T. Kishimoto, M.

- Ueda and S. Inouye, Coherent Transfer of Photoassociated Molecules into the Rovibrational Ground State, *Phys. Rev. Lett.*, 105 (2010), 203001.
- [34] E. S. Sachs, J. Hinze and N. H. Sabelli, MCSCF calculations for six states of NaH, *J. Chem. Phys.*, 62 (1975), 3367.
- [35] E. S. Sachs, J. Hinze and N. H. Sabelli, Transition moments, band strengths, and line strengths for NaH, *J. Chem. Phys.*, 62 (1975), 3384.
- [36] T.-S. Chu, Y. Zhan and K.-L. Han, The time-dependent quantum wave packet approach to the electronically nonadiabatic processes in chemical reactions, *Int. Rev. Phys. Chem.*, 25 (2006), 201.
- [37] P.-F. Lan, E. J. Takahashi, K.-L. Liu, Y.-X. Fu and K. Midorikawa, Carrier envelope phase dependence of electron localization in the multicycle regime, *New J. Phys.*, 15 (2013), 063023.
- [38] P.-F. Lan, E. J. Takahashi and K. Midorikawa, Efficient control of electron localization by subcycle waveform synthesis, *Phys. Rev. A*, 86 (2012), 013418.
- [39] K.-L. Liu, Q.-B. Zhang and P.-X. Lu, Enhancing electron localization in molecular dissociation by two-color mid- and near-infrared laser fields, *Phys. Rev. A*, 86 (2012), 033410.